

Pseudo-mutant P53 is a unique phenotype of *DNMT3A*-mutated pre-leukemia

Amos Tuval,^{1,2} Yardena Brilon,¹ Hadas Azogy,^{1,3} Yoni Moskovitz,¹ Dena Leshkowitz,⁴ Tomer M Salame,⁴ Mark D Minden,^{5,6,7,8} Perry Tal,⁹ Varda Rotter,⁹ Moshe Oren,⁹ Nathali Kaushansky¹ and Liran I Shlush^{1,10,11}

¹Department of Immunology, Weizmann Institute of Science, Rehovot, Israel; ²Department of Hematology, Meir Medical Center, Kfar Saba, Israel; ³Department of Pathology, Sackler Faculty of Medicine, Tel Aviv University, Tel Aviv, Israel; ⁴Department of Life Sciences Core Facilities, Weizmann Institute of Science, Rehovot, Israel; ⁵Princess Margaret Cancer Center, University Health Network (UHN), Toronto, Ontario, Canada; ⁶Department of Medicine, University of Toronto, Toronto, Ontario, Canada; ⁷Division of Medical Oncology and Hematology, University Health Network, Toronto, Ontario, Canada; ⁸Department of Medical Biophysics, University of Toronto, Toronto, Ontario, Canada; ⁹Department of Molecular Cell Biology, Weizmann Institute of Science, Rehovot, Israel; ¹⁰Division of Hematology, Rambam Health Care Campus, Haifa, Israel and ¹¹Molecular Hematology Clinic, Maccabi Healthcare Services, Tel Aviv, Israel

Correspondence: L. I. Shlush
liran.shlush@weizmann.ac.il

Received: November 9, 2021.
Accepted: January 19, 2022.
Prepublished: February 24, 2022.

<https://doi.org/10.3324/haematol.2021.280329>

©2022 Ferrata Storti Foundation
Published under a CC BY-NC license 

Abstract

Pre-leukemic clones carrying *DNMT3A* mutations have a selective advantage and an inherent chemoresistance, however the basis for this phenotype has not been fully elucidated. Mutations affecting the gene *TP53* occur in pre-leukemic hematopoietic stem/progenitor cells (preL-HSPC) and lead to chemoresistance. Many of these mutations cause a conformational change and some of them were shown to enhance self-renewal capacity of preL-HSPC. Intriguingly, a misfolded P53 was described in AML blasts that do not harbor mutations in *TP53*, emphasizing the dynamic equilibrium between wild-type (WT) and “pseudo-mutant” conformations of P53. By combining single cell analyses and P53 conformation-specific monoclonal antibodies we studied preL-HSPC from primary human *DNMT3A*-mutated AML samples. We found that while leukemic blasts express mainly the WT conformation, in preL-HSPC the pseudo-mutant conformation is the dominant. HSPC from non-leukemic samples expressed both conformations to a similar extent. In a mouse model we found a small subset of HSPC with a dominant pseudo-mutant P53. This subpopulation was significantly larger among *DNMT3A*^{R882H}-mutated HSPC, suggesting that while a pre-leukemic mutation can predispose for P53 misfolding, additional factors are involved as well. Treatment with a short peptide that can shift the dynamic equilibrium favoring the WT conformation of P53, specifically eliminated preL-HSPC that had dysfunctional canonical P53 pathway activity as reflected by single cell RNA sequencing. Our observations shed light upon a possible targetable P53 dysfunction in human preL-HSPC carrying *DNMT3A* mutations. This opens new avenues for leukemia prevention.

Introduction

Although acute myeloid leukemia (AML) is preceded by clonal hematopoiesis (CH), most CH clones are not “pre-leukemic” and do not transform to AML.¹ When referring to the most common mutated gene in CH, *DNMT3A*, the main discriminative characteristics between pre-AML and CH are larger clones and more accompanying mutations, reflecting the selective advantage of these clones.² Experimental and clinical studies have demonstrated that *DNMT3A*-mutated pre-leukemic clones have also an inherent chemoresistance and the ability to reconstitute the bone marrow following AML chemotherapeutic treatments.³⁻⁵ The mechanisms behind this pre-AML phenotype remain unclear.

Mutations affecting *TP53* occur during the pre-leukemic stage of AML.⁶ Some of these mutations cause a conformational change⁷ that can be detected using conformation-specific monoclonal antibodies.⁸ In a heterozygous state, the mutant protein can have a dominant negative effect over the wild-type (WT) protein that leads to chemoresistance and P53 dysfunction as reflected by a reduced expression of downstream target genes of P53.⁹ Moreover, *TP53* mutations can enhance the self-renewal capacity of murine hematopoietic stem/progenitor cells (HSPC).¹⁰ Interestingly, a dynamic equilibrium was described between the WT and the mutant conformations of P53. The WT protein can acquire a “pseudo-mutant” conformation

rendering it dysfunctional, with a reduced transcriptional activity¹¹. The pseudo-mutant conformation was found in TP53 WT AML blasts,¹² and was correlated with growth factor stimulation.¹³

In this report we investigated whether P53 conformational changes occur during early evolutionary stages of DNMT3A-mutated (TP53 WT) AML, similar to the stages during which TP53 mutations appear. Furthermore, we tested the influence of a short peptide, that stabilizes the WT conformation of P53 and restores its transcriptional activity,¹⁴ on the fitness of DNMT3A-mutated pre-leukemic HSPC (preL-HSPC) *in vivo*. This was performed by assessing its influence on their engraftment capacity in immuno-deficient mice.

Methods

Samples

Primary samples were received from Princess Margaret Cancer Center, University Health Network (UHN), Canada (UHN IRB protocol 01-0573) and from Rambam Health Care Campus, Israel (IRB protocol #283-1). Clinical characteristics of each sample are presented in the *Online Supplementary Table S1*.

Mass cytometry

We analyzed primary AML samples with mass cytometry using a panel of metal-conjugated monoclonal antibodies targeting surface markers (*Online Supplementary Table S2A*) and P53 conformation-specific monoclonal antibodies that were conjugated to heavy metals: PAb1620 (for the WT conformation) and PAb240 (for the mutant conformation). The antibody staining concentrations were determined by titration on positive and negative control cell populations. Specifically, intra-nuclear antibody concentrations were calibrated using MCF 7 cells line (TP53 WT) and RXF 393 cell line (TP53^{R175H}) (*Online Supplementary Figure S1*). Absence of false positive staining was validated using HL-60 cell line (TP53 null). All samples were stained and recorded at least in duplicates (except for the mobilized peripheral blood mononuclear cell [PBMC] donations, due to paucity of available cells). See the *Online Supplementary Appendix* for details.

Xenotransplantation assays and *in vivo* pharmacologic treatment

All experiments were performed in accordance with Institutional Guidelines approved by the Weizmann Institute of Science Animal Care Committee (11790319-2) and as described previously³. Primary CD3-depleted AML samples were injected to immune-deficient mice (see the *Online Supplementary Appendix* for additional information). Five weeks after the injection of human cells, when engraftment was established, we treated some of the mice for 2 weeks

with pCAP-250 (myr- RRHSTPHPD)¹⁴. Other mice were treated with a scrambled, control peptide. Mice were sacrificed on day 56. We evaluated human engraftment by flow cytometry and sorted the main sub-populations for deep targeted DNA sequencing according to the mutations of the original injected pool, thus identifying their stem cell of origin (Figure 4A) (see the *Online Supplementary Appendix*).

Single cell RNA sequencing and mass cytometry of engrafting cells

Following mice sacrifice and bone marrows retrieval (from the injected and non-injected bones), cells from all mice of each treatment cohort were pooled together. Human cells were separated according to the expression of human CD45 (EasySep™, StemCell Technologies, Vancouver, Canada) (Figure 5). The lack of murine cells was validated by flow cytometry using human-specific antibodies (*Online Supplementary Table S3*). Alignment of single cell RNA sequencing (scRNA-seq) data to murine genome excluded any contamination with murine cells (see the *Online Supplementary Appendix*). Viable cells (Trypan Blue negative) were divided as follows: 5x10⁶ cells from each cohort were taken for mass cytometry and 100,000 cells from each cohort were taken for scRNA-seq. 40,000 cells of CD3 depleted cells of the original, injected, sample (PBMC) were also taken for scRNA-seq alongside the engrafting cells. Mass cytometry was performed using antibody panel shown in the *Online Supplementary Tables S2B* and *S2C*. scRNA-seq libraries were prepared using 10X Genomics technology (see the *Online Supplementary Appendix*).

Mass cytometry of DNMT3A^{R882H} mouse model of clonal hematopoiesis

Following mice sacrifice, bone marrows were extracted and enriched for Lin- cells (EasySep™, StemCell Technologies, Vancouver, Canada). Mass cytometry was performed using antibody panel shown in the *Online Supplementary Table S2D*, using the same staining protocol. PAb1620 and PAb240 detect both murine and human P53.

Statistical analyses

Comparisons between two groups, were performed using the two-tailed, non-paired, non-parametric Wilcoxon rank sum test with 95% confidence interval (CI) and continuity correction.

Results

P53 conformations in DNMT3A-mutated, TP53 wild-type leukemic blasts and pre-leukemic hematopoietic stem/progenitor cells

In order to determine P53 conformations in leukemic blasts and in preL-HSPC we analyzed by mass cytometry nine

DNMT3A-mutated, *TP53* WT, *NPM1c* human AML samples. We chose this AML subtype because it is the most common subtype representing 15% of AML clones¹⁵ and because the ability to clearly distinguish between leukemic blasts (harboring both *DNMT3A* and *NPM1* mutations) and pre-leukemic cells (harboring only *DNMT3A* mutations).

All samples underwent deep sequencing to verify that they do not carry *TP53* mutations even at low variant allele frequencies (VAF). Leukemic blasts from each AML sample were gated according to the immune-phenotype that was originally reported by the clinical laboratory of the medical center where patients were diagnosed (which appears next to each sample in the *Online Supplementary Table S1*).

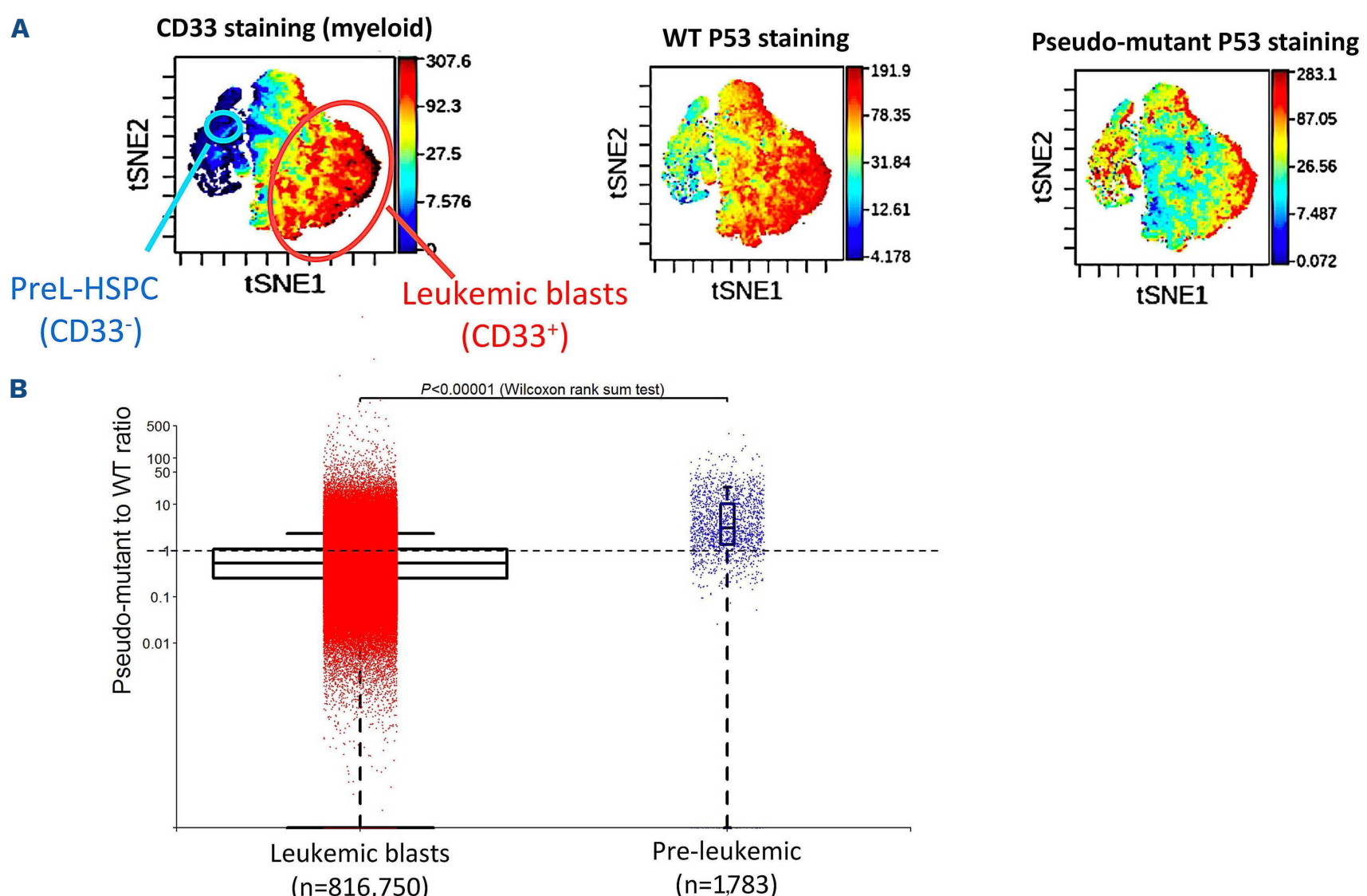
Phenotypic preL-HSPC were defined as cells that are negative for CD33, CD15, CD11b, CD19, CD79b, CD3, CD16 and CD45RA and are CD34-positive. When identified in primary AML samples, a portion of the cells with this immune-phenotype were shown to be pre-leukemic (harboring only *DNMT3A* mutation, without *NPM1* mutation).³

We found that blasts expressed high levels of P53, most of it in its WT conformation (Figure 1A). Nonetheless, the pseudo-mutant conformation was present as well as previously described.¹²

Next, we calculated the ratio between the intensity of the two conformations of P53 in each individual cell. We termed

this ratio the “pseudo-mutant to WT conformation ratio”, PM/WT-CR. We found that, although there is wide variability with regard to the expression of the two conformations of P53, leukemic blasts express mainly the WT conformation (with a median PM/WT-CR of 0.53) while phenotypic preL-HSPC express mainly the pseudo-mutant conformation of P53 (a median PM/WT-CR of 3.06) (Figure 1B). Since staining with PAb240 and PAb1620 is mutually exclusive,^{16,17} the sum of their intensities gives an estimate of the total P53 expression in each cell. PreL-HSPC with a high PM/WT-CR had higher levels of total P53 when compared with PreL-HSPC with a low PM/WT-CR (*Online Supplementary Figure S2*), similar to *TP53*-mutated cells in myelodysplastic syndromes.¹⁸

The misfolded conformation of P53, that reacts with the monoclonal antibody PAb240, can be induced by cytokines,¹³ temperature¹⁹ or hypoxia.²⁰ We therefore, studied cells that were frozen immediately after they were collected from peripheral blood, without exposing them to culture media or cytokines. All staining procedures and sample handling were performed in a temperature of 20°C (lower than the temperature range that can cause p53 misfolding¹⁹) and not under hypoxic conditions. Since the PAb240 antibody we used, can react also with a denatured P53, we verified that our staining procedure does not



Continued on following page.

Figure 1. Mass cytometry of primary human acute myeloid leukemia samples. Single cell analysis of primary human acute myeloid leukemia (AML) samples was performed by mass cytometry. P53 conformation-specific monoclonal antibodies were used to measure the level of expression of each P53 conformation: PAb1620 for the wild-type (WT) conformation and PAb240 for the mutant (or misfolded) conformation. Sub-populations that reside in the samples were identified by a panel of monoclonal antibodies targeting surface markers. Hematopoietic stem/progenitor cells (HSPC) were defined as having CD45RA⁻ CD33⁻ CD19⁻ CD79b⁻ CD15⁻ CD16⁻ CD11b⁻ CD3⁻ immuno-phenotype. (A) A representative viSNE analysis of mass cytometry single cell data showing CD33 staining (left panel) in the peripheral blood of a *DNMT3A^{R882H}*, *NPM1c* AML patient. As expected, most cells are leukemic blasts (circled in red). The high resolution of mass cytometry allowed the identification of rare phenotypic pre-leukemic HSPC as well (circled in blue). P53 staining superimposed on the same viSNE analysis (middle and right panels) demonstrate that blasts express mainly the WT conformation of P53, while the dominant conformation in pre-leukemic cells is the pseudo-mutant conformation. (B) The ratio between the intensity of the pseudo-mutant conformation and that of the WT conformation of P53 was calculated for each cell of 9 AML samples. Each dot represents a single cell. n denotes the number of cells analyzed in each cell population. The dashed line represents equal intensities of both conformations (ratio of 1). In each of these cell populations there is variability with regard to the expression of the two conformations of P53. However, in the leukemic blasts (red), the dominant conformation is the WT with a median ratio of 0.53. In the pre-leukemic cells (blue) the dominant conformation of P53 is the pseudo-mutant, with a ratio of 3.06. Box plot centers, hinges and whiskers represent the median, first and third quartiles and 1.5 X interquartile range, respectively. Boxes are drawn with widths proportional to the square-roots of the number of observations in each group. The two-tailed, non-paired, non-parametric Wilcoxon rank sum test was used with 95% confidence interval and continuity correction. tSNE: t-distributed stochastic neighbor-embedding.

cause significant denaturation of P53 by testing it in *TP53* WT cell line (*Online Supplementary Figure S1*). The fact that different samples and different cells within samples presented with different levels of PAb240 staining (with some being negative for this staining), attest for lack of P53 denaturation during the staining process. Other reports, that have identified almost exclusively the pseudo-mutant conformation in AML blasts,¹² used a less gentle intra-cellular staining protocol than us.

P53 conformations in cord blood and in *DNMT3A*-mutated non-pre-leukemic hematopoietic stem/progenitor cells

In order to understand whether the high expression level of the pseudo-mutant conformation of P53 is part of a more general stem cell phenotype, we used the same immune-phenotypic criteria and analyzed CD34⁺-enriched cells of a healthy cord blood sample.

Both conformations of P53 were detected in all sub-populations, however in contrast to preL-HSPC, cord blood HSPC expressed them to a similar extent (*Online Supplementary Table S14*). At the single cell level, cord blood HSPC had a significantly lower PM/WT-CR (a median PM/WT-CR of 1.22 in cord blood HSPC compared with a median PM/WT-CR of 3.06 in preL-HSPC, $P<0.00001$, Wilcoxon rank sum test, Figure 2A).

We further analyzed two samples of mobilized PBMC donated by individuals with *DNMT3A^{R882H}*-mutated CH with high VAF of 19.7% and 34% (*Online Supplementary Table S1*). Both samples had no other additional mutations as assessed by our sequencing panel. Here too, we noticed variability at the single cell level, however HSPC from these non-leukemic *DNMT3A^{R882H}*-mutated samples were found to have a median PM/WT-CR of 0.53, significantly lower than in preL-HSPC ($P<0.00001$, Wilcoxon rank sum test, Figure 2A). Figure 2B emphasizes the inter-sample and intra-sample heterogeneity. In most primary AML samples, preL-HSPC have a high PM/WT-CR.

P53 conformations in non-*DNMT3A*-mutated pre-leukemic hematopoietic stem/progenitor cells

We studied a *TP53^{R248Q}*-mutated AML sample (#161632) without any *DNMT3A* mutations. R248Q substitution causes destabilization of P53⁷ and disrupts P53's transcriptional activity.^{21,22} However, it causes only a partial misfolding of P53¹⁹ and was found to have a relatively weak reactivity with PAb240.^{16,21,23} As expected, most CD33⁺ blasts had a stronger reactivity with PAb1620 (*Online Supplementary Figure S3*). These blasts have lost their WT *TP53* allele (having del(17) by conventional G-band analysis, and *TP53^{R248Q}* VAF of 94%, *Online Supplementary Table S1*), confirming the weak reactivity of *TP53^{R248Q}* with PAb240. In contrast, phenotypic preL-HSPC had a stronger reactivity with PAb240 than with PAb1620 (median PAb1620 to PAb240 ratio of 2.1, Figure 2B far right). It is conceivable that these cells have a residual WT *TP53* allele,^{24,25} emphasizing that their increased reactivity with PAb240 might reflect the presence of a "pseudo-mutant" P53.

P53 conformations in LSK cells of a *DNMT3A^{R882H}* clonal hematopoiesis mouse model

We studied Lin⁻ Sca-1⁺ cKit⁺ cells (analogous to human HSPC) derived from a rodent model of *DNMT3A^{R882H}* clonal hematopoiesis. We crossed the human *DNMT3A^{R882H}* knock-in mice²⁶ with mice carrying a Cre recombinase allele under the regulation of Vav promotor which is expressed only in the hematopoietic system²⁷ to create hematopoietic-specific human *DNMT3A* mutant mice (h*DNMT3A^{R882H}*). C57Bl x Vav-Cre mice were used as a control group (Cre-control). We also used *DNMT3A* haplo-insufficient mice (m*Dnmt3a* haploinsufficiency) that model *DNMT3A* frameshift mutations. All mice were males.

We sacrificed four male mice (one of each genotype) at 11.5 months ("wild-type" [WT]) to 22 months of age ("m*Dnmt3a* haploinsufficiency").

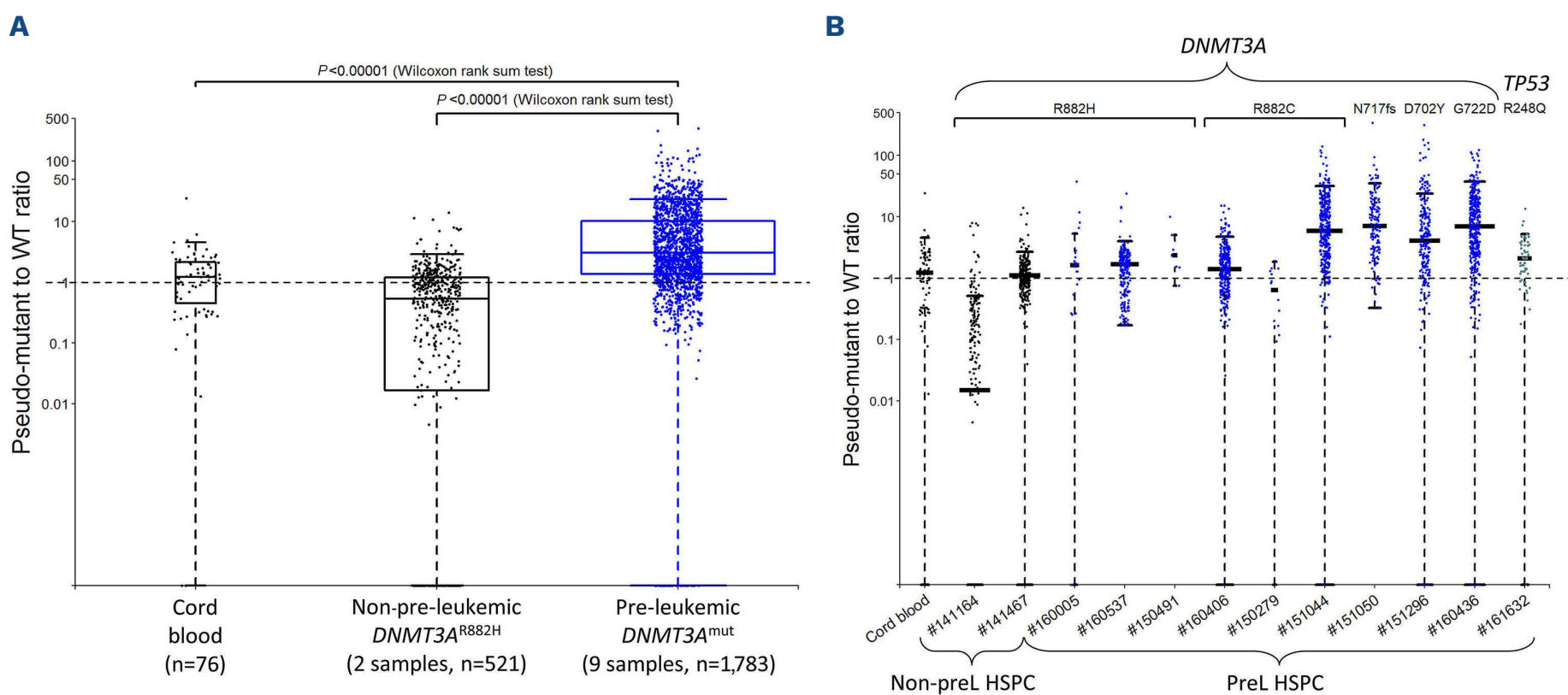


Figure 2. Mass cytometry of human hematopoietic stem/progenitor cells from leukemic and non-leukemic samples. Immunophenotypic hematopoietic stem and progenitor cells (HSPC) from a cord blood sample and from two *DNMT3A*^{R882H}-mutated mobilized peripheral blood mononuclear cell (PBMC) samples were analyzed by mass cytometry. All cells that are CD45RA⁻ CD33⁻ CD19⁻ CD79b⁻ CD15⁻ CD16⁻ CD11b⁻ CD3⁻ were included. The ratio between the intensity of the pseudo-mutant conformation and that of the wild-type (WT) conformation of P53 was calculated for each cell. Each dot represents a single cell. (A) The pseudo-mutant to WT conformation ratio was around or below 1 in non-leukemic HSPC, significantly lower than that measured in pre-leukemic HSPC (preL-HSPC) (n denotes their number in each sample cohort). The dashed line represents equal intensities of both conformations (ratio of 1). Box plot centers, hinges and whiskers represent the median, first and third quartiles and 1.5 X interquartile range, respectively. Boxes are drawn with widths proportional to the square-roots of the number of observations in each group. The two-tailed, non-paired, nonparametric Wilcoxon rank sum test was used with 95% confidence interval and continuity correction. (B) Because of the variability at the single cell level with regard to the expression of the two conformations of P53, data for each individual sample are presented separately. The specific *DNMT3A* or *TP53* variant appears above each sample. From left to right: HSPC from a cord blood sample, HSPC from 2 samples of *TP53*-WT, *DNMT3A*^{R882H}-mutated clonal hematopoiesis (all in black), HSPC from 9 *TP53*-WT, *DNMT3A*-mutated AML samples (blue), HSPC from a *DNMT3A*-WT, *TP53*^{R248Q}-mutated AML sample (light blue). In 8 of 9 preL-HSPC samples the dominant conformation of P53 is the pseudo-mutant. Although the *TP53*^{R248Q} variant has low reactivity with PAb240, pre-leukemic cells of this sample demonstrated a high PAb240 to PAb1620 intensity ratio, similar to other preL-HSPC, implying the possible presence of a “pseudo-mutant” conformation of their residual *TP53*-WT allele (see text for details). The median and 1.5 X interquartile range are presented for each sample. The medians are drawn proportional to the square-roots of the number of observations in each cohort.

We found that although the median values of the PM/WT-CR in all mouse genotypes were less than 1 (P53 is mainly in its WT conformation), h*DNMT3A*^{R882H} mice had significantly more LSK cells with an extremely high PM/WT-CR. 82 cells (4.9%) of h*DNMT3A*^{R882H} LSK cells had a PM/WT-CR greater than 10, significantly more than the 17 (0.9%) WT LSK cells with this high ratio ($P < 0.0001$, Chi-square test of independence with Yates continuity correction, Figure 3).

All LSK cells were found to be in G0 (as assessed by combined cyclin B1 and KI-67 staining, *Online Supplementary Table S2D*), even those with this extremely high PM/WT-CR.

Targeting P53 mutant conformation in vivo

We speculated that the high PM/WT-CR can contribute to the enhanced selective advantage of preL-HSPC^{10,28} and that reverting this ratio might reduce their fitness. We

chose to explore this by using patient-derived xenograft models. In these models, the human cells are injected to and engraft immuno-deficient mice. The murine environment exerts a selective pressure on the injected cells, exposing different stem cells that reside in them. In about a third of mice, that are injected with PBMC donated by AML patients at the time of diagnosis, the engrafting human cells are enriched with progeny of preL-HSPC (determined by sequencing the engrafting cells).^{3,6} This model can be utilized also to assess the sensitivity of the engrafting cells (as reflected by their engraftment and differentiation capacities) to various therapeutic interventions (Figure 4A). As a model for an intervention that can target a high PM/WT-CR, we used a short peptide (myr-RRHSTPHPD, named: pCAP-250) that can shift the balance between the WT and the mutant conformations of P53 by stabilizing the WT conformation. This peptide was shown to restore the downstream transcriptional activity of P53.¹⁴

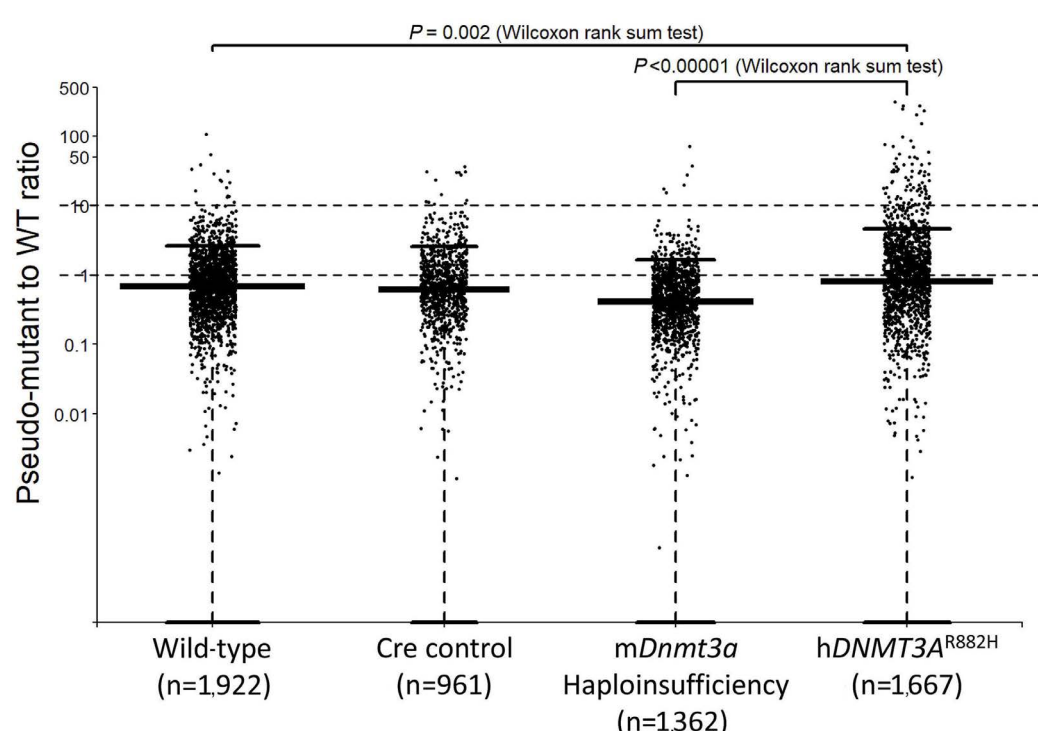


Figure 3. P53 conformations in murine LSK cells. Immunophenotypic LSK cells of a mouse model of human *DNMT3A*^{R882} clonal hematopoiesis. Samples were analyzed by mass cytometry. The ratio between the intensity of the pseudo-mutant conformation and that of the wild-type (WT) conformation of P53 was calculated for each cell. Each dot represents a single cell. n denotes the number of cells in each sample. The dashed lines at ratios 1 and 10 represent equal intensities of both conformations and high levels of the pseudo-mutant conformation, respectively. 82 cells (4.9%) of h*DNMT3A*^{R882H}-mutated LSK cells had a conformation ratio greater than 10, significantly more than the 17 (0.9%) WT LSK cells with this high ratio ($P<0.0001$, Chi-square test of independence between genotype and number of LSK cells with a conformation ratio greater than 10, with Yates continuity correction). Comparisons between total LSK cells retrieved from the different mice were performed using a two-tailed, non-paired, non-parametric Wilcoxon rank sum test with 95% confidence interval and continuity correction. Medians values are: WT: 0.7; Cre control: 0.61; m*Dnmt3a* haplo-insufficient: 0.41; h*DNMT3A*^{R882H}: 0.81. The median and 1.5 X interquartile range are presented for each sample. The medians are drawn proportional to the square-roots of the number of observations in each cohort.

We tested the influence of pCAP-250 on the engraftment capacity of the above-mentioned *DNMT3A*, *NPM1* mutated AML samples (that their preL-HSPC express pseudo-mutant P53). Most samples resulted in non-pre-leukemic human grafts (either leukemic engraftments or non-pre-leukemic, multi-lineage engraftments). However, one sample (sample #160005) that its preL-HSPC express mainly the pseudo-mutant conformation of P53 (Figure 2B), gave rise to a multi-lineage graft (*Online Supplementary Figure S4*) that was composed of pre-leukemic cells harboring only the pre-leukemic *DNMT3A* mutation (*Online Supplementary Table S7*). The engraftment capacity of these cells decreased significantly following treatment with pCAP-250 in three independent experiments (Figure 4B). pCAP-250 treatment did not affect the engraftment capacity of cord blood, non-preL-HSPC from an AML sample, *DNMT3A*^{R882H} CH or of leukemic stem cells (Figure 4C to F, *Online Supplementary Tables S8 to S10*).

Molecular characterization of cells affected by P53-directed therapeutic intervention

We wanted to explore P53 conformations and its transcriptional activity in the engrafting pre-leukemic cells by studying them with mass cytometry and scRNA-seq, respectively. In order to achieve this, we injected the AML sample that gave rise to a pre-leukemic graft (sample

#160005) into recipient mice, treated the mice with a single dose of pCAP-250 at 8 weeks, sacrificed the mice 12 hours later and analyzed the engrafting human cells by both methodologies (Figure 5).

We performed unbiased clustering of the mass cytometry data of engrafting cells (100,000 cells of each treatment cohort) according to their surface markers. We found that there was no qualitative difference between the two treatment cohorts: mice treated with pCAP-250 and mice treated with the control peptide engrafted with the same human sub-populations (clusters) as shown in Figure 6A. However, in accordance with the decreased engraftment observed in Figure 4B, some clusters decreased quantitatively in the treated mice. This quantitative difference was significantly dependent on treatment cohort ($P<0.000001$, chi square test of independence). Performing a post hoc standardized residuals analysis (with a Bonferroni correction for multiple comparisons) revealed that among the clusters that decreased quantitatively in treated mice, clusters 1, 3, 4, 8, 9, 14 and 19 (Figure 6B), are the source of that difference (*Online Supplementary Table S15*). Most cells that belong to these clusters were eliminated in the pCAP-250 treated mice. It is therefore possible that cells extracted from pCAP-250 treated mice represent resistant cells. In order to characterize cells that are sensitive to pCAP-250 treatment, we decided to

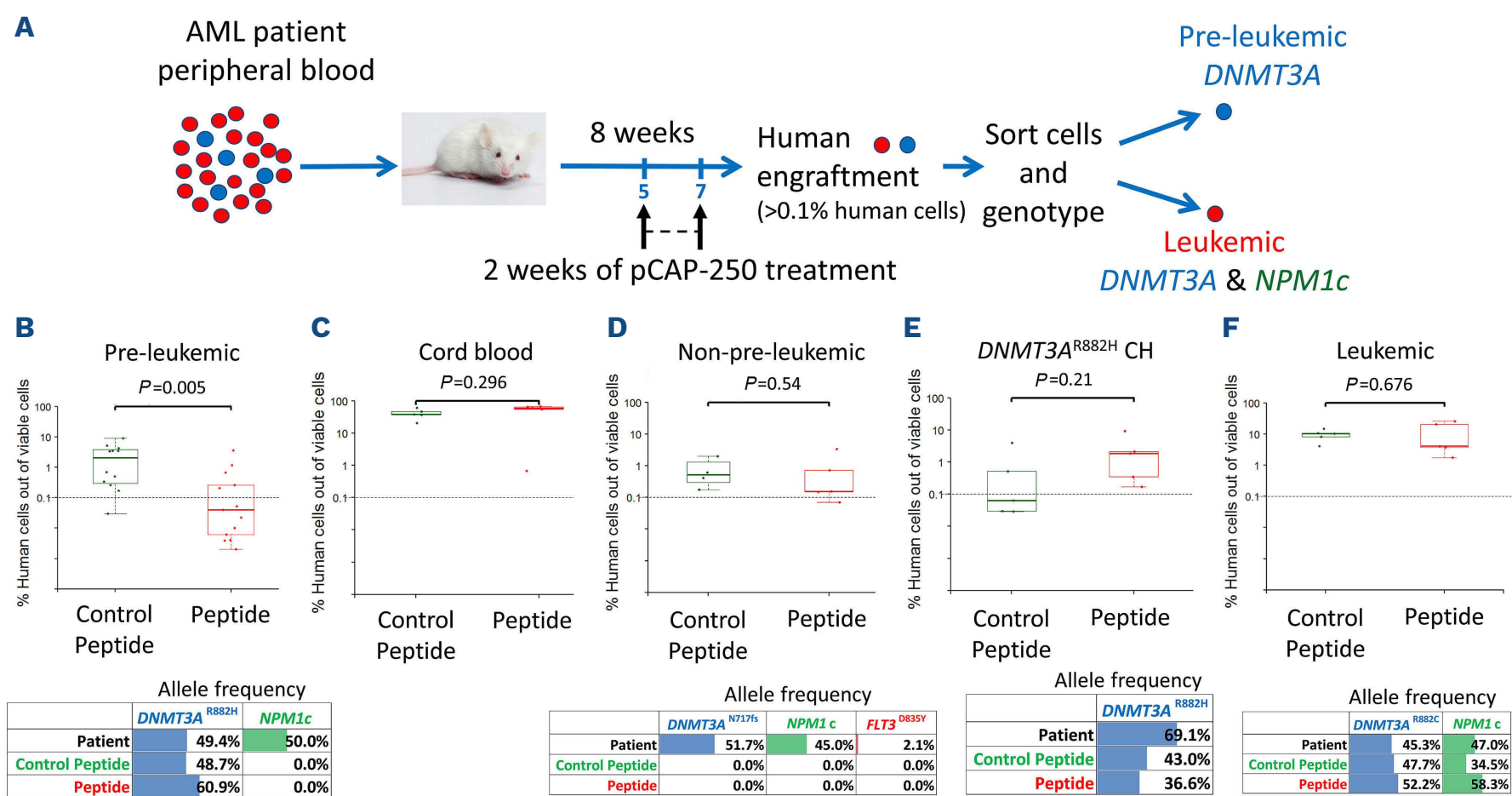


Figure 4. Xenotransplantation assays and in vivo pharmacologic treatment. (A) Schematic of the experimental setup. The pool of peripheral blood mononuclear cells (PBMC) of acute myeloid leukemia (AML) patients contains mainly blasts (red circles) but also rare pre-leukemic hematopoietic stem and progenitor cells, preL-HSPC (blue circles). Sorting and sequencing the engrafting cells allowed us to determine whether they originate from preL-HSPC (having only a *DNMT3A* mutation) or from leukemic stem cells (having both *DNMT3A* and *NPM1* mutations). This experimental model enabled us to explore the sensitivity of the different cells to P53-directed treatment. (B to F) Engraftment of the different injected samples as assessed by flow cytometry according to treatment cohort: control peptide (green) and pCAP-250 treated (peptide, red). Each dot represents a mouse and the dashed line represents the threshold for engraftment (presence of 0.1% of human cells out of all cells extracted from the bone marrow). The origin of the engrafting cells was determined by sequencing. Below each plot appear the medians of the allele frequency of *DNMT3A* and *NPM1* mutations in the injected sample (patient) and in the engrafting cells retrieved from mice in each cohort (control peptide and peptide) attesting for their stem cell of origin. CH: clonal hematopoiesis (detailed sequencing results are presented in the *Online Supplementary Tables S7 to S10*). Box plot centers, hinges and whiskers represent the median, first and third quartiles and 1.5 X interquartile range, respectively. Boxes are drawn with widths proportional to the square-roots of the number of observations in each cohort. All comparisons were performed using a two-tailed, non-paired, non-parametric Wilcoxon rank sum test with 95% confidence interval and continuity correction.

examine the median intensities of surface markers and of P53 conformations in cells that belong to these clusters and that were extracted from the control peptide treated mice. These clusters showed mainly a myeloid/monocytic differentiation pattern although some had low expression of B cell lineage markers (*Online Supplementary Table S11*). The ratio between the two conformations of P53 in most engrafting cells was lower than that measured in the injected HSPC and was around 1 (Figure 6C). There was no correlation between clusters of cells that quantitatively decreased following pCAP-250 treatment and the PM/WT-CR of their cells. However, cells in the clusters that were quantitatively affected the most by pCAP-250 treatment (clusters 14 and 19, *Online Supplementary Table S15*) had a high PM/WT-CR (Figure 6C) and these clusters contained 90% and 79% such cells, respectively (*Online Supplementary Table S11*). Our scRNA-seq data validated the pre-leukemic stem cell origin of the engrafting cells: unbiased clustering that was performed for all samples together (patient PBMC and en-

grafting cells) presented the monomorphic nature of the leukemic blasts (represented by only 4 clusters, none of which was found among the engrafting cells) in contrast to the 22 different clusters that represent the engrafting cells (*Online Supplementary Figure S5*). Additionally, somatic variant calling of the scRNA-seq data identified only the *DNMT3A*^{R882H} mutation in the engrafting cells, without the *NPM1c* mutation.

Similar to the mass cytometry data, the scRNA-seq data revealed that engrafting cells from both treatment cohorts contained the same subpopulations (clusters) and that not all clusters decreased quantitatively to a similar extent in the treated cohort. Clusters 0,2,5,13 and 20 decreased quantitatively (*Online Supplementary Table S12*), and this decrease from 46.4% to 29.6%, was found to be significantly dependent on treatment cohort ($P<0.021$) (Figure 7A).

Gene expression of these clusters was found to be enriched with genes that are related to B cell differentiation

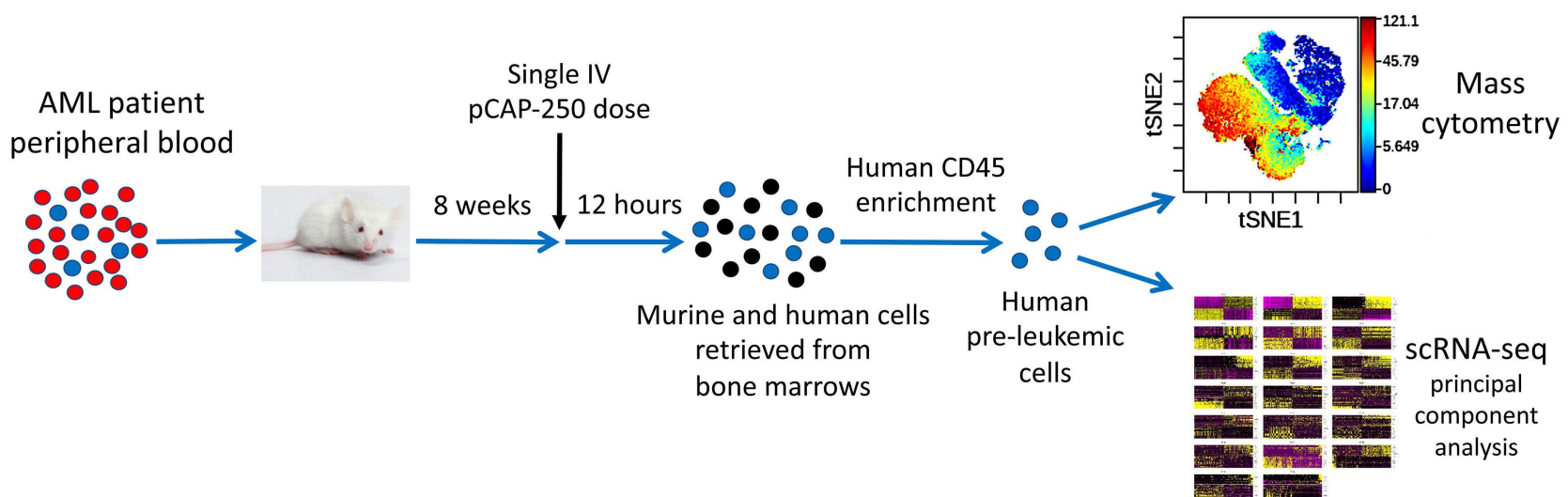


Figure 5. P53 conformations and transcriptional activity in engrafting pre-leukemic cells. Schematic of the experimental setup for P53 conformation analyses by mass cytometry and for gene expression profiling by single cell RNA sequencing (scRNA-seq) of engrafting human cells. Acute myeloid leukemia (AML) sample #160005 that contains mainly blasts (red circles) but also rare pre-leukemic hematopoietic stem/progenitor cells (preL-HSPC) (blue circles) was injected to NSG immune-deficient mice. This sample produces pre-leukemic human grafts harboring the *DNMT3A* mutation without the mutation in *NPM1*. At 8 weeks a single dose of pCAP-250 or the control peptide (16.6 mg/kg) was administered intravenously (IV) to the recipient mice and mice were sacrificed 12 hours later. Cells retrieved from bone marrows of all mice in each treatment cohort were pooled together and murine hematopoietic cells (black circles) were depleted using human CD45 enrichment kit. Human pre-leukemic cells (blue circles) were divided between downstream analyses methodologies (as detailed in the *Online Supplementary Appendix* and the methods sections). tSNE: t-distributed stochastic neighbor-embedding.

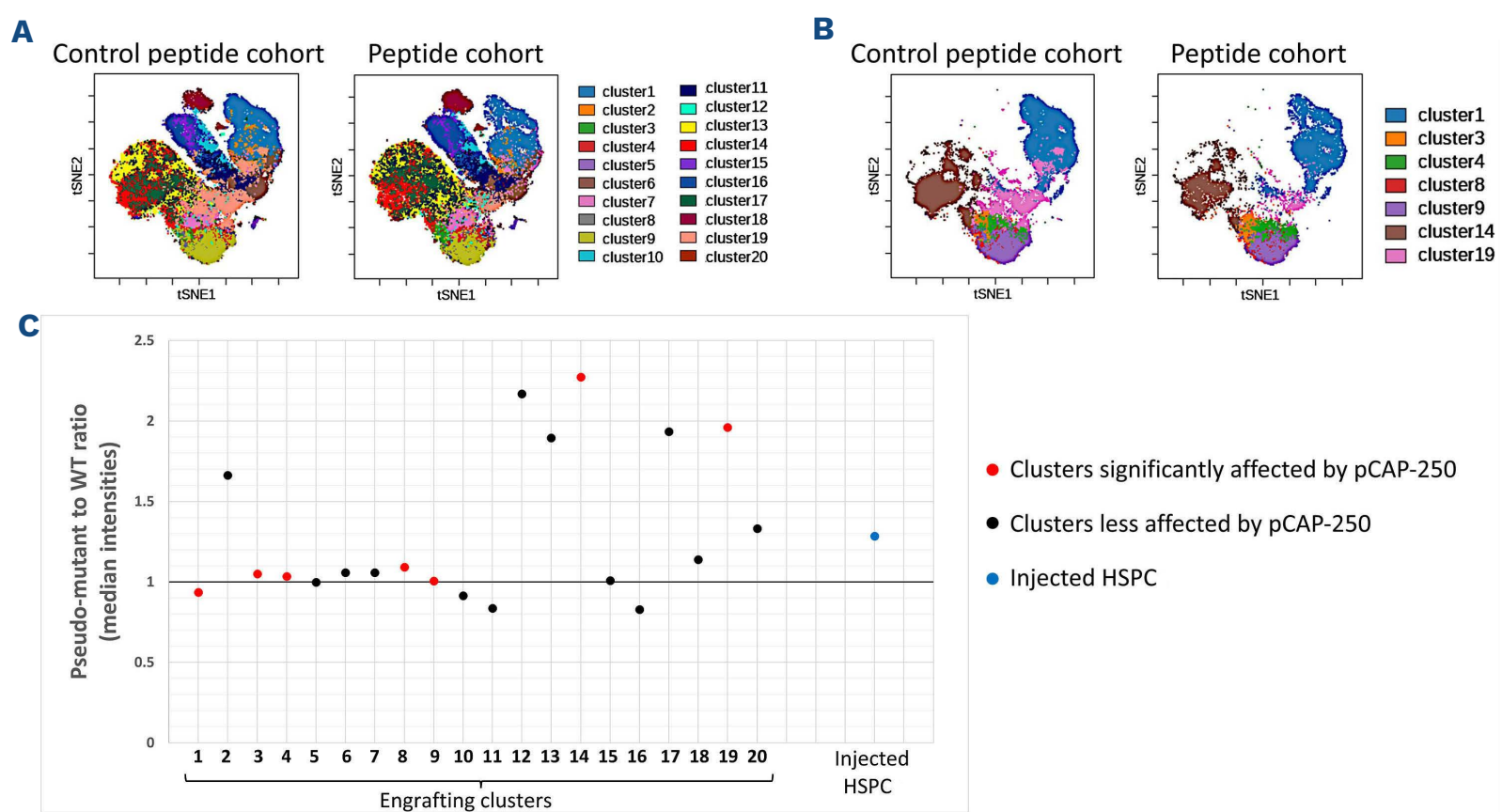


Figure 6. Mass cytometry of engrafting cells. All positively stained surface markers were used for unbiased clustering (FlowSOM analysis) of the mass cytometry data of engrafting cells. WT: wild-type; HSPC: hematopoietic stem and progenitor cells. (A) All clusters. (B) Clusters with a significant quantitative decrease following treatment with pCAP-250 (*Online Supplementary Table S15*). (C) Ratio of the median intensities of the pseudo-mutant and WT conformations of P53 (PM/WT-CR) in engrafting cells and in the injected HSPC. Engrafting cells (from control peptide treated mice) are categorized by the clusters shown in (A). Data about injected HSPC were obtained from sample #160005 as shown in Figure 2B.

(cluster 0), to MAPK and NFkB pathways (cluster 2), and to monocyte differentiation and Interferon signaling pathway (cluster 13) (similar to the mass cytometry data, *Online Supplementary Table S11*).

Gene expression of less affected clusters was found to be enriched with genes that are related to B-cell differenti-

ation (clusters 1), to macrophage/monocyte differentiation (cluster 6), to mast cell/basophil differentiation (cluster 18) and to plasmacytoid/dendritic differentiation (cluster 21) (*Online Supplementary Table S13*). The similarities in expression of differentiation markers and genes between affected clusters and less-affected clusters mean that

pCAP-250 treatment did not cause a differentiation bias. Analyzing the cell cycle score of the clusters that were affected by pCAP-250 treatment revealed that they are mainly in G1 phase (Figure 7B). This means that the treatment was not specifically affecting proliferating cells. Cells in the clusters that decreased quantitatively following treatment with pCAP-250 had a significantly reduced expression of *CDKN1A* (P21), relative to their *TP53* expression level ($P<0.006$, Figure 7C). Apart from this reduction in *CDKN1A* expression, we did not identify any additional reduced expression of other P53-regulated genes,²⁹ thus a pseudo-mutant P53 could have a partial P53-transcriptional dysfunction, similar to other *TP53* mutants.³⁰ In summary, cells affected by pCAP-250 were not characterized by their differentiation or proliferation signatures, but rather by their P53 function.

We tried to understand how the cells were eliminated in the pCAP-250 treated mice. We did not find an increase in apoptosis, necroptosis (*RIPK1* or *RIPK3*) or ferroptosis pathway genes in pCAP-250 treated samples when compared to control samples. Nonetheless, the clusters that decreased following pCAP-250 treatment had a reduced

expression of *CD44* and of *GPX4* when compared with other clusters.

Targeting TP53 mutant in vivo

In order to test the sensitivity of *TP53*-mutant cells to pCAP-250, we injected peripheral blood mononuclear cells of the *TP53^{R248Q}*-mutated AML sample described above (#161632), to immune-deficient mice and then treated them with pCAP-250 (single dose at week 8). The overall engraftment capacity of the human cells was not influenced by the treatment (Figure 8A). When we analyzed by flow cytometry the engrafting sub-populations, we found that most engrafting cells have a myeloid immune-phenotype (Figure 8B, green and brown colors) similar to the injected blasts, suggesting that most of them originate in leukemic stem cells. Nevertheless, we did see small subpopulations of engrafting cells with a non-myeloid immune-phenotype, mainly in the control cohort (Figure 8B, blue colors). Although not verified by targeted sequencing, this points to engraftment of pre-leukemic stem cells, preferentially in the control cohort. We therefore speculated that pCAP-250 specifically elim-

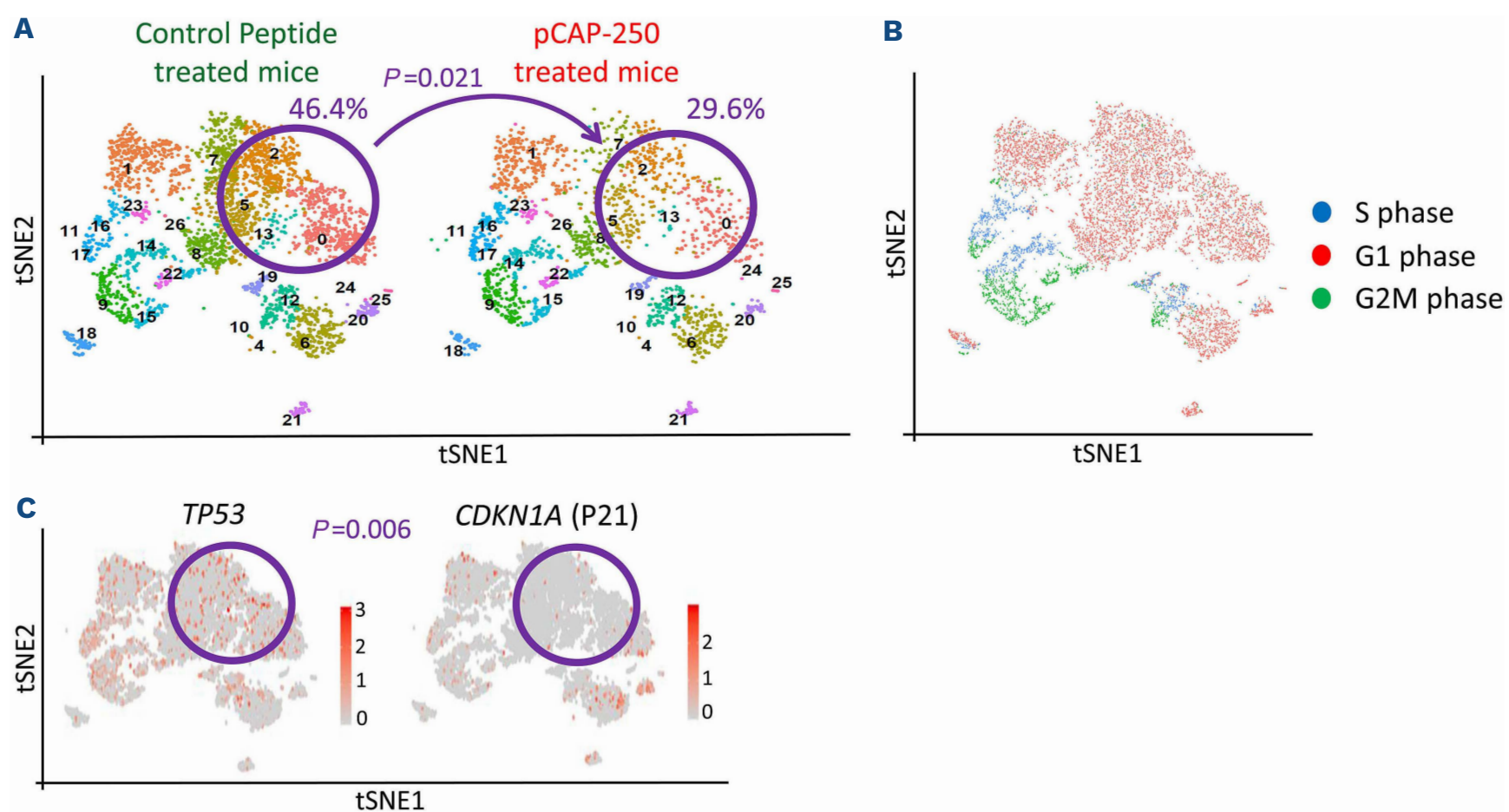
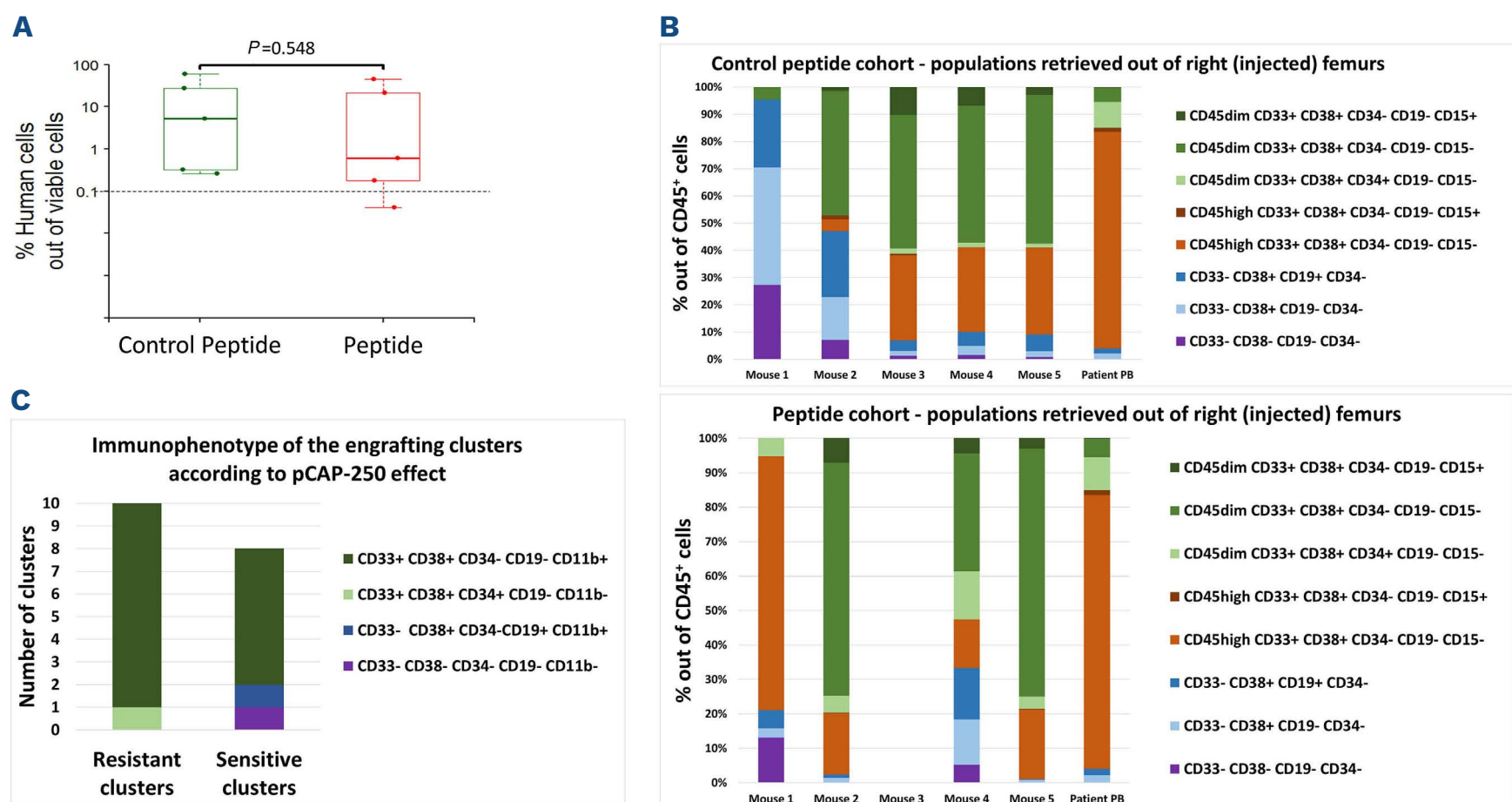


Figure 7. Single cell RNA sequencing of engrafting cells. (A) tSNE (t-distributed stochastic neighbor-embedding) analyses of single cell RNA sequencing (scRNA-seq) data of engrafting cells. Each dot represents a cell. Both treatment cohorts contain the same sub-populations, however, some clusters (0, 2, 5, 13 and 20 that are circled in purple) decreased quantitatively following treatment with pCAP-250. This decrease from 46.4% to 29.6%, was found to be significantly dependent on treatment cohort ($P<0.021$, chi square test of independence with Yates continuity correction). (B) Cell cycle score of engrafting cells from both the “control peptide” and “peptide” cohorts superimposed on the tSNE analyses shown in (A). Most cells in pCAP-250-affected clusters belong to the “control peptide” cohort. (C) tSNE analyses of scRNA-seq data of engrafting cells with the expression of *TP53* (left) and of *CDKN1A* (P21, right). We calculated the difference between the logarithmic fold change of the expression of *CDKN1A* and that of *TP53* in pCAP-250-affected cells (clusters 0, 2, 5, 13) and compared it to the same difference that was calculated for less affected cells (clusters 1, 6–9, 12, 14–19, 21–23). We found that affected cells had a significantly reduced expression of *CDKN1A* relative to their *TP53* expression, when compared to other clusters of cells ($P=0.006$, Wilcoxon rank sum test).

inated these subpopulations in the treated cohort. In order to test this, we pooled together engrafting cells from all mice in each cohort (as described in the methods section) and analyzed them by mass cytometry using the antibody panel shown in the *Online Supplementary Table S2C*. This panel included two anti-mouse monoclonal antibodies that allowed us to “gate out” any residual murine cells. We then performed an unbiased clustering of 247,300 engrafting cells from each treatment cohort, according to their surface markers. A significant difference that was dependent on treatment cohort was found between the control sample and the treated sample ($P<0.000001$, chi square test of independence). Performing a *post hoc* standardized residuals analysis (with a Bonferroni correction for multiple testing) revealed that clusters 4,5,6,7,9,10,11 and 15 that quantitatively decreased in the treated mice (sensitive to pCAP-250), and clusters 1, 8, 12, 13, 14, 16, 17, 18, 19 and 20 that quantitatively increased in the treated mice (resistant to pCAP-250) are the source of that difference. While all the resistant clusters had a leukemic immune-phenotype (Figure 8C, green colors), the non-myeloid clusters (clusters 4 and 11 in the *Online Supplementary Table S16*, Figure 8C, purple and blue, respectively) were found to be sensitive to pCAP-250 treatment (*Online Supplementary Table S16* and *S17*), consistent with our flow cytometry analysis (Figure 8B). Indeed, some of the sensitive clusters have a myeloid immune-phenotype (Figure 8C, green), however, these too might have a pre-leukemic origin (as shown in the *Online Supplementary Table S7*, peptide-treated cohort, mouse #5).

Discussion

In this work, we studied P53 conformations in human cells representing several steps along AML evolutionary trajectory. We focused on the most common pre-leukemic mutation, in the *DNMT3A* gene^{1,2} and therefore our conclusions are limited to *DNMT3A*-mutated preL-HSPC. We observed that *DNMT3A*-mutated preL-HSPC had significantly higher PM/WT-CR in comparison to AML blasts, to normal cord blood and to HSPC of *DNMT3A*-mutated CH (Figures 1B and 2A). Next, we demonstrated that preL-HSPC carrying *DNMT3A* mutations were sensitive to treatment with a small peptide targeting the dynamic equilibrium between P53 conformations (pCAP-250)¹⁴ (Figure 4B). Single cell RNA-sequencing analyses of treated cells suggested that human preL-HSPC that are sensitive to pCAP-250 had a reduced expression of P21, the major canonical downstream target of P53. Altogether, these findings suggest that the dominant conformation of P53 in preL-HSPC carrying *DNMT3A* mutations is the pseudo-mutant conformation and at least some of them, that exhibit dysfunctional P53 transcriptional activity, could be sensitive to perturbations in the balance between P53 conformations. While our study provides evidence for a dominant pseudo-mutant P53 conformation in *DNMT3A*-mutated preL-HSPC, and to some degree dysfunctional P53 transcriptional activity, it remains unclear whether these phenotypes functionally contribute to chemo-resistance and increased fitness (the hallmarks of *DNMT3A*-mutated preL-HSPC^{3-5,31-36}). In order to answer this question, we used patient-de-



Continued on following page.

Figure 8. pCAP-250 treatment of a TP53^{R248Q} acute myeloid leukemia patient-derived xenograft model. NSG-SGM3 mice were injected with *TP53^{R248Q}* acute myeloid leukemia (AML) (#161632) sample and treated by a single dose of pCAP-250 8 weeks later. (A) Engraftment of human cells (percentages of human CD45⁺ cells as assessed by flow cytometry) according to treatment cohort: control peptide (green) and pCAP-250-treated (peptide, red). The overall engraftment was not affected by pCAP-250 treatment. Each dot represents a mouse and the dashed line represents the threshold for engraftment (presence of 0.1% of human cells out of all cells extracted from the bone marrow). Box plot centers, hinges and whiskers represent the median, first and third quartiles and 1.5 X interquartile range, respectively. Boxes are drawn with widths proportional to the square-roots of the number of observations in each cohort. All comparisons were performed using a two-tailed, non-paired, non-parametric Wilcoxon rank sum test with 95% confidence interval and continuity correction. (B) Flow cytometry analyses of the engrafting sub-populations in the control (upper panel) and treated (lower panel) cohorts. Injected peripheral blood mononuclear cells (PBMC) appear in the right bars (Patient PB). Only human CD45⁺ cells that were extracted from the right femurs of the mice are presented. PB: peripheral blood. Most engrafting cells are myeloid (green and brown colors), similar to the injected blasts (right bars), reflecting their leukemic origin. Some non-myeloid sub-populations are seen as well (blue colors), reflecting their differentiation capacity and their non-leukemic origin. The control cohort is enriched with these, non-myeloid, sub-populations when compared with the treated cohort. (C) Immunophenotype of engrafting clusters following FlowSOM analysis (unbiased clustering) of the mass cytometry data of the engrafting human cells. Clusters are grouped according to their sensitivity to pCAP-250 treatment: “resistant” clusters are clusters with a quantitative increase following pCAP-250 treatment and “sensitive” clusters are clusters with a quantitative decrease following pCAP-250 treatment. The number of clusters in each group is presented. All 10 resistant clusters have a leukemic immunophenotype (green colors, similar to the leukemic blasts). Of note, one of the resistant clusters (cluster 8 in the *Online Supplementary Table S17*) has a CD33⁺CD38⁺CD34⁺ immunophenotype (light green). It probably represents leukemic cells because among the injected blasts a small sub-population with these markers was identified (panel B, right bars). The non-myeloid clusters (clusters 4 and 11 in the *Online Supplementary Table S16*, purple and blue, respectively) are present only among the sensitive clusters, in line with our flow cytometry analyses (panel B). Six of 8 sensitive clusters have a myeloid immunophenotype (green), however, it is possible that they have a pre-leukemic origin (as in the *Online Supplementary Table S7*, peptide-treated cohort, mouse #5).

rived xenograft experiments and treatment with pCAP-250.

These experiments revealed that treatment with pCAP-250 diminished the engraftment capacity of preL-HSPC (Figure 4B) reflecting a reduction in self-renewal capacity at the stem or progenitor cell level. Most of the sensitive cells were eliminated, and therefore could not be studied directly. In order to overcome this, we performed unbiased clustering analyses for both the pCAP-250-treated and the control peptide-treated cells together. By doing so, we were able to characterize the sensitive cells using data from the control-peptide cohort. We identified clusters of cells that were influenced by pCAP-250 treatment (clusters 14 and 19, Figure 6B and C; *Online Supplementary Table S15*) and demonstrated that the vast majority of their cells (80-90%) expressed P53 predominantly in its pseudo-mutant conformation. Engrafting cells that were selectively eliminated by pCAP-250 treatment had a high ratio between their P53 expression and their P21 expression levels (Figure 7A and C). Since P21 is the major canonical *TP53*-regulated gene, these cells had a partially dysfunctional P53 canonical pathway and as mentioned above, some of them had a high PM/WT-CR. These results can be explained by additional factors influencing the conformation equilibrium of P53 or by other mechanisms by which pCAP-250 eliminates cells, however they could also point to possible functional consequences of a high PM/WT-CR of P53 that should be further explored in the future.

Non-R882 *DNMT3A* variants are more prevalent in CH than in AML,³⁷ and when such clones transform to AML, they are accompanied by a lower number of cooperating mutations.³⁸ This implies that single mutant clones carrying

non-R882 *DNMT3A* mutations have enhanced self-renewal when compared with single mutant clones carrying *DNMT3A^{R882}* mutations (that undergo rapid clonal expansion after they acquire additional mutations). Figure 2B demonstrates that *DNMT3A^{R882}*-mutated cells might have a lower PM/WT-CR when compared with cells harboring non-R882 variants of *DNMT3A*, and although our study is not statistically powered to draw any definite conclusions, this does support a possible correlation between a high PM/WT-CR and increased self-renewal capacity.

In order to gain more support to our claim that increased PM/WT-CR and dysfunctional P53 activity are associated with the increased fitness and progression of *DNMT3A*-mutated preL-HSPC we treated with pCAP-250 both cord blood samples and HSPC from healthy individuals carrying *DNMT3A* mutations (CH). We could not identify reduced engraftment after treatment with pCAP-250. Furthermore, the PM/WT-CR of both CH and cord blood derived HSPC was lower than preL-HSPC. In this regard it is important to stress that preL-HSPC derived from AML patients might be phenotypically different from HSPC carrying *DNMT3A* from the CH stage. While we know that individuals with large clones (with a variant allele frequency of more than 10%, reflecting their enhanced fitness) have high (50%) chances to evolve to AML,² we do not understand the evolutionary trajectory (epigenetically due to accumulation of methylation changes and phenotypically) of the HSPC that eventually transform to AML.

Altogether, we were able to demonstrate that P53-directed treatment, that is capable of stabilizing the WT conformation of P53,¹⁴ specifically targeted *DNMT3A*-mutated human preL-HSPC and possibly also *TP53*-mutated preL-HSPC. This was demonstrated in two samples, thus we cannot

generalize our conclusions, but it suggests that at least some of the fitness advantage of preL-HSPC is correlated with the presence of pseudo-mutant P53.

Despite this limitation it is clear from our study that *DNMT3A*-mutated preL-HSPC have a high PM/WT-CR. Our *hDNMT3A^{R882H}* mouse model data emphasize that a pre-leukemic mutation (*DNMT3A^{R882H}* in this case) predisposes P53 in a subpopulation of HSPC to acquire a pseudo-mutant conformation. Similar to our observations of a high PM/WT-CR among cells that belong to an early developmental stage of malignancy, high levels of pseudo-mutant P53 were reported in other pre-malignant states,³⁹ and P53 dysfunction was detected in *DNMT3A*-mutated pre-malignant thymocytes.⁴⁰ Future studies might shed light on the molecular mechanisms that underlie this phenotype.

It was recently shown that *DNMT3A*-mutated HSPC have enhanced self-renewal under inflammatory conditions.⁴¹ Previous studies have demonstrated that cytokines,¹³ and inflammation³⁹ can modulate P53's folding and that a misfolded P53 characterizes leukemic blasts with enhanced self-renewal.²⁸ An inflammatory environment, as present in the serum of AML patients,⁴² might modify P53 conformations and lead to a higher PM/WT-CR. However, we found that leukemic blasts that share the same cytokine-rich environment have the lowest levels of pseudo-mutant P53. It was previously suggested that mutant conformation of P53 is correlated with cell proliferation.⁴³ Our data (produced by using methodologies with a higher resolution and including more cells) do not support this claim (Figure 7B, *DNMT3A^{R882H}* murine LSK cells with a high PM/WT-CR being in G0). Other factors besides inflammation or the mutational profile of the clone (as implied by our findings in *TP53^{R248Q}*-mutated preL-HSPC) could also induce a pseudo-mutant P53. For example: the cellular proteomic composition,¹¹ P53's interactions with other proteins,^{44,45} zinc chelation,⁴⁶ oxidative stress,⁴⁷ P53's ubiquitination (PAb240 recognizes an MDM2-bound P53)⁴⁸ the silencing of Hippo tumor suppressor pathway⁴⁹ were all implicated in the conformational switch of P53. It is possible that interactions between the environment and the pre-leukemic clone are responsible for the higher PM/WT-CR observed in *DNMT3A*-mutated preL-HSPC, and future studies can expose such an etiology.

In summary, our observations in human preL-HSPC highlight a unique phenotype that characterizes part of the pre-leukemic clone. Interestingly, *DNMT3A*-mutated primary AML do not present with a classical *TP53*-mutated phenotype (namely, a complex karyotype) suggesting that the pseudo-mutant P53 is not equivalent to a mutated P53.

Realizing that the enhanced self-renewal of pre-leukemic cells could be correlated with their P53 protein folding and not only with their mutational profile calls for studying the physiological and pathological mechanisms that induce this conformational change (whether cell-intrinsic or micro-environmental factors). It remains unclear whether this phenomenon can be generalized to other (non-*DNMT3A*) pre-leukemic mutations or other pre-malignant conditions and whether it could be exploited for targeting these pre-malignant clones. However, it can potentially open new avenues for both AML prediction and for its prevention.

Disclosures

PT, VR and MO are founders of Quintrigen.

Contributions

VR, MO and LS initiated the project; AT, NK and LS designed the research, and wrote the paper with input from other authors; AT, NK, HA and YM performed the research; AT, YB, DL and TMS analyzed the data; MDM contributed clinical samples; PT contributed reagents and cell lines.

Acknowledgments

The authors would like to thank Andrea Arruda for providing the clinical information of the primary samples and to Merav Kedmi from the Department of Life Sciences core facilities at the Weizmann Institute of Science for technical guidance.

Funding

This research was supported by the EU horizon 2020 grant project MAMLE ID: 714731, LLS and rising tide foundation grant ID: RTF6005-19, ISF-NSFC 2427/18, ISF-IPMP-Israel Precision Medicine Program 3165/19, BIRAX 713023, the Ernest and Bonnie Beutler Research Program of Excellence in Genomic Medicine, awarded to LIS. LIS is an incumbent of the Ruth and Louis Leland career development chair. NK is an incumbent of the Applebaum Foundation Research Fellow Chair. This research was also supported by the Sagol Institute for Longevity Research, the Barry and Eleanore Reznik Family Cancer Research Fund, Steven B. Rubenstein Research Fund for Leukemia and Other Blood Disorders, the Rising Tide Foundation and the Applebaum Foundation.

Data sharing statement

The dataset generated and analyzed during the current study are available in the NCBI Sequence Read Archive (SRA; <https://www.ncbi.nlm.nih.gov/sra/>) under access numbers. Code is available on GitHub under <https://github.com/ShlushLab>

References

1. Jaiswal S, Fontanillas P, Flannick J, et al. Age-related clonal hematopoiesis associated with adverse outcomes. *N Engl J Med.* 2014;371(26):2488-2498.
2. Abelson S, Collard G, Ng SWK, et al. Prediction of acute myeloid leukaemia risk in healthy individuals. *Nature.* 2018;559(7714):400-404.
3. Shlush LI, Zandi S, Mitchell A, et al. Identification of pre-leukaemic haematopoietic stem cells in acute leukaemia. *Nature.* 2014;506(7488):328-333.
4. Guryanova OA, Shank K, Spitzer B, et al. DNMT3A mutations promote anthracycline resistance in acute myeloid leukemia via impaired nucleosome remodeling. *Nat Med.* 2016;22(12):1488-1495.
5. Jongen-Lavrencic M, Grob T, Hanekamp D, et al. Molecular minimal residual disease in acute myeloid leukemia. *N Engl J Med.* 2018;378(13):1189-1199.
6. Lal R, Lind K, Heitzer E, et al. Somatic TP53 mutations characterize preleukemic stem cells in acute myeloid leukemia. *Blood.* 2017;129(18):2587-2591.
7. Bullock AN, Henckel J, Dedecker BS, et al. Thermodynamic stability of wild-type and mutant p53 core domain. *Proc Natl Acad Sci USA.* 1997;94(26):14338-14342.
8. Gannon JV, Greaves R, Iggo R, et al. Activating mutations in p53 produce a common conformational effect. A monoclonal antibody specific for the mutant form. *EMBO J.* 1990;9(5):1595-1602.
9. Boettcher S, Miller PG, Sharma R, et al. A dominant-negative effect drives selection of TP53 missense mutations in myeloid malignancies. *Science.* 2019;365(6453):599-604.
10. Chen S, Wang Q, Yu H, et al. Mutant p53 drives clonal hematopoiesis through modulating epigenetic pathway. *Nat Commun.* 2019;10(1):5649.
11. Trinidad AG, Muller PAJ, Cuellar J, et al. Interaction of p53 with the CCT complex promotes protein folding and wild-type p53 activity. *Mol Cell.* 2013;50(6):805-817.
12. Zheng A, Castren K, Säily M, et al. p53 status of newly established acute myeloid leukaemia cell lines. *Br J Cancer.* 1999;79(3/4):407-415.
13. Zhang W, Deisseroth AB. Conformational change of p53 protein in growth factor-stimulated human myelogenous leukemia cells. *Leuk Lymphoma.* 1994;14(3-4):251-255.
14. Tal P, Eizenberger S, Cohen E, et al. Cancer therapeutic approach based on conformational stabilization of mutant P53 protein by small peptides. *Oncotarget.* 2016;7(11):11817-11837.
15. Papaemmanuil E, Gerstung M, Bullinger L, et al. Genomic classification and prognosis in acute myeloid leukemia. *N Engl J Med.* 2016;374(9):2209-2221.
16. Chen S, Wu JL, Liang Y, et al. Arsenic trioxide rescues structural p53 mutations through a cryptic allosteric site. *Cancer Cell.* 2021;39(2):225-239.
17. Milner J. Flexibility: the key to p53 function? *Trends Biochem Sci.* 1995;20(2):49-51.
18. Saft L, Karimi M, Ghaderi M, et al. p53 protein expression independently predicts outcome in patients with lower-risk myelodysplastic syndromes with del(5q). *Haematologica.* 2014;99(6):1041-1049.
19. Bullock AN, Henckel J, Fersht AR. Quantitative analysis of residual folding and DNA binding in mutant p53 core domain: definition of mutant states for rescue in cancer therapy. *Oncogene.* 2000;19(10):1245-1256.
20. Gogna R, Madan E, Kuppusamy P, Pati U. Chaperoning of mutant p53 protein by wild-type p53 protein causes hypoxic tumor regression. *J Biol Chem.* 2012;287(4):2907-2914.
21. Ory K, Legros Y, Auguin C, Soussi T. Analysis of the most representative tumour-derived p53 mutants reveals that changes in protein conformation are not correlated with loss of transactivation or inhibition of cell proliferation. *EMBO J.* 1994;13(15):3496-3504.
22. Kotler E, Shani O, Goldfeld G, et al. A systematic p53 mutation library links differential functional impact to cancer mutation pattern and evolutionary conservation. *Mol Cell.* 2018;71(1):178-190.
23. Rodrigues NR, Rowan A, Smith ME, et al. p53 mutations in colorectal cancer. *Proc Natl Acad Sci U S A.* 1990;87(19):7555-7559.
24. Wong TN, Ramsingh G, Young AL, et al. Role of TP53 mutations in the origin and evolution of therapy-related acute myeloid leukaemia. *Nature.* 2015;518(7540):552-555.
25. Bernard E, Nannya Y, Hasserjian RP, et al. Implications of TP53 allelic state for genome stability, clinical presentation and outcomes in myelodysplastic syndromes. *Nat Med.* 2020;26(10):1549-1556.
26. Scheller M, Ludwig AK, Göllner S, et al. Hotspot DNMT3A mutations in clonal hematopoiesis and acute myeloid leukemia sensitize cells to azacytidine via viral mimicry response. *Nat Cancer.* 2021;2:527-544.
27. Joseph C, Quach JM, Walkley CR, Lane SW, Lo Celso C, Purton LE. Deciphering hematopoietic stem cells in their niches: a critical appraisal of genetic models, lineage tracing, and imaging strategies. *Cell Stem Cell.* 2013;13(5):520-533.
28. Zhu YM, Bradbury D, Russell N. Expression of different conformations of p53 in the blast cells of acute myeloblastic leukaemia is related to in vitro growth characteristics. *Br J Cancer.* 1993;68(5):851-855.
29. Andrysik Z, Galbraith MD, Guarnieri AL, et al. Identification of a core TP53 transcriptional program with highly distributed tumor suppressive activity. *Genome Res.* 2017;27(10):1645-1657.
30. Van Nguyen T, Puebla-Osorio N, Pang H, Dujka ME, Zhu C. DNA damage-induced cellular senescence is sufficient to suppress tumorigenesis: a mouse model. *J Exp Med.* 2007;204(6):1453-1461.
31. Cole CB, Russler-Germain DA, Ketkar S, et al. Haploinsufficiency for DNA methyltransferase 3A predisposes hematopoietic cells to myeloid malignancies. *J Clin Invest.* 2017;127(10):3657-3674.
32. Lindsley RC, Mar BG, Mazzola E, et al. Acute myeloid leukemia ontogeny is defined by distinct somatic mutations. *Blood.* 2015;125(9):1367-1376.
33. Wong TN, Miller CA, Klco JM, et al. Rapid expansion of preexisting nonleukemic hematopoietic clones frequently follows induction therapy for de novo AML. *Blood.* 2016;127(7):893-897.
34. Höllein A, Meggendorfer M, Dicker F, et al. NPM1 mutated AML can relapse with wild type NPM1: persistent clonal hematopoiesis can drive relapse. *Blood Adv.* 2018;2(22):3118-3125.
35. Krönke J, Bullinger L, Teleanu V, et al. Clonal evolution in relapsed NPM1-mutated acute myeloid leukemia. *Blood.* 2013;122(1):100-108.
36. Chen J, Matatall KA, Feng X, et al. Dnmt3a-null hematopoietic stem and progenitor cells expand after busulfan treatment. *Exp Hematol.* 2020;91:39-45.
37. Buscarlet M, Provost S, Feroz Zada Y, et al. DNMT3A and TET2

- dominate clonal hematopoiesis, demonstrate benign phenotypes and different genetic predisposition. *Blood*. 2017;130(6):753-762.
38. Miles LA, Bowman RL, Merlinsky TR, et al. Single-cell mutation analysis of clonal evolution in myeloid malignancies. *Nature*. 2020;587(7834):477-482.
39. Kodama M, Murakami K, Okimoto T, Sato R, Watanabe K, Fujioka T. Expression of mutant type-p53 products in H pylori-associated chronic gastritis. *World J Gastroenterol*. 2007;13(10):1541-1546.
40. Haney SL, Upchurch GM, Opavska J, et al. Dnmt3a Is a Haploinsufficient Tumor Suppressor in CD8+ Peripheral T Cell Lymphoma. *PLoS Genet*. 2016;12(9):e1006334.
41. Liao M, Chen R, Yang Y, et al. Aging-elevated inflammation promotes DNMT3A R878H-driven clonal hematopoiesis. *Acta Pharm Sin B*. 2022;12:678-691.
42. Sanchez-Correa B, Bergua JM, Campos C, et al. Cytokine profiles in acute myeloid leukemia patients at diagnosis: Survival is inversely correlated with IL-6 and directly correlated with IL-10 levels. *Cytokine*. 2013;61(3):885-891.
43. Bi S, Lanza F, Goldman JM. The Involvement of "tumor suppressor" p53 in normal and chronic myelogenous leukemia hemopoiesis. *Cancer Res*. 1994;54(2):582-586.
44. Hainaut P, Milner J. Interaction of heat-shock protein 70 with p53 translated in vitro: evidence for interaction with dimeric p53 and for a role in the regulation of p53 conformation. *EMBO J*. 1992;11(10):3513-3520.
45. Rivlin N, Katz S, Doody M, et al. Rescue of embryonic stem cells from cellular transformation by proteomic stabilization of mutant p53 and conversion into WT conformation. *Proc Natl Acad Sci USA*. 2014;111(19):7006-7011.
46. Hainaut P, Milner J. A structural role for metal ions in the "wild-type" conformation of the tumor suppressor protein p53. *Cancer Res*. 1993;53(8):1739-1742.
47. Hainaut P, Milner J. Redox modulation of p53 conformation and sequence-specific DNA binding in vitro. *Cancer Res*. 1993;53(19):4469-4473.
48. Sasaki M, Nie L, Maki CG. MDM2 binding induces a conformational change in p53 that is opposed by heat-shock protein 90 and precedes p53 proteasomal degradation. *J Biol Chem*. 2007;282(19):14626-14634.
49. Furth N, Bossel Ben-Moshe N, Pozniak Y, et al. Down-regulation of LATS kinases alters p53 to promote cell migration. *Genes Dev*. 2015;29(22):2325-2330.